High-Field/High-Frequency ESR Study of Gd@C_{82}-I

Ko Furukawa,[†] Shingo Okubo,[§] Haruhito Kato,[‡] Hisanori Shinohara,[‡] and Tatsuhisa Kato*[,†,§]

Institute for Molecular Science, Nishigo-naka 38, Myodaiji, Okazaki 444-8585, Japan, Department of Chemistry, Nagoya University, Nagoya 464-8602, Japan, and The Graduate University for Advanced Studies, Hayama, Kanagawa 240-0193, Japan

Received: July 7, 2003; In Final Form: September 16, 2003

The spin state of the major isomer of Gd@C_{82} (Gd@C_{82}-I) was determined by the combined use of a high-field electron spin resonance (ESR) spectrometer (W-band) and a conventional spectrometer (X-band). The ground spin state of Gd@C_{82}-I is characterized by an integer spin quantum number of $S = 3$. The spin ($S = 1/2$) on the π orbital of the fullerene cage is coupled with the octet spin ($S = 7/2$) of the encapsulated gadolinium in an antiferromagnetic manner with the exchange coupling constant of $J = -1.8$ cm^{-1}. In a condensed solution and solid powder, the Gd@C_{82}-I molecules easily formed dimers. The radical spins on the cage are canceled upon dimerization, and the resultant spin state of the dimer is described by two independent octet ($S = 7/2$) spins of the gadolinium. The X- and W-band ESR spectra for Gd@C_{82}-I are completely reproduced by an eigenfield method simulation, and ESR parameters for the **g** tensor, zero-field splitting tensor, and the intramolecular exchange coupling constant, *J*, have been determined. From the temperature dependence of the W-band ESR spectrum, the sign of the zero-field splitting constant *D* has been determined to be positive.

Introduction

Recently, much attention has been paid to endohedral metallofullerene, which encapsulates metal atoms in fullerene cages. The metallofullerenes containing a variety of transition and lanthanide metals have been reported.[1−15] Gd@C_{82} is of particular interest because of the relationship with fullerenol Gd@$C_{82}(OH)_n$[16,17] and Gd@C_{82} peapod,[18,19] which have potential for medical and nanotechnological applications. Gd@C_{82} molecules have been isolated by many scientists.[20−22] The molecular structure of Gd@C_{82}-I was identified as having C_{2v} symmetry from the observation of the similarity of the absorption spectrum with that for La@C_{82}-I.[23] It has been reported that this system is described as "$Gd^{3+}@C_{82}^{3-}$", which results from the charge transfer from the Gd atom to the C_{82} cage.[24] The electronic configuration of a Gd atom is [Xe]$6s^2 4f^7 5d^1$, and it is proposed that the three electrons on the outer 6s and 5d orbitals are transferred to the π^* orbital of the C_{82} cage in the process of the encapsulation. As a result, a radical spin is produced on the C_{82} cage. This radical spin on the C_{82} cage plays an important role in the spin structure with respect to the magnetic interaction with the Gd^{3+} spin. Funasaka et al. have reported the temperature dependence of the magnetic susceptibility of Gd@C_{82}.[25,26] They conclude that the spin structure of the Gd@C_{82} is characterized by the spin quantum number $S = 7/2$ due to seven electrons on the Gd^{3+} ion. Huang et al. obtained the temperature dependence of the magnetic susceptibility for Gd@C_{82},[27,28] which was consistent with the report by Funasaka et al. They proposed that the effective magnetic moment at room temperature corresponds to the $S = 3$ state arising from the antiparallel arrangement between the Gd and the radical spin on C_{82} cage; however, the detailed measurement on the spin state of Gd@C_{82} has never been reported. Sanakis et al. have investigated the related molecules Er@C_{82}-I and II by dual-mode X-band ESR spectroscopy, in which the microwave field was perpendicularly and parallel polarized toward the static magnetic field.[29] They analyzed the ESR spectra under the effective spin quantum number approximation, and suggested that there are different exchange interactions between the Er@C_{82}-I and -II. The analogous study of Gd@C_{82} has not been reported, because it is difficult to analyze the ESR spectrum for reasons mentioned below.

The radical electron on the C_{82} cage exerts an influence on the dimer formation of metallofullerenes. Hasegawa et al. reported the preferential dimer formation of Y@C_{82} along the step of the Cu(III) 1×1 surface under vacuum using a scanning tunneling microscope.[30] They concluded that the Y@C_{82} molecule is one of the first cases of the so-called "super-atom", which was originally proposed for semiconductor heterostructures. It can be generally considered that the dimer is a unit of cluster growth in the case of metallofullerenes.

In this investigation, magnetic properties of the major isomer of Gd@C_{82} (Gd@C_{82}-I (C_{2v})) are examined using ESR spectroscopy. The zero-field splitting of the Gd^{3+} ions is generally as large as the X-band (9.5 GHz) microwave energy. In this case, the spectrum analysis is not straightforward, since the ESR spectra for these systems become very asymmetric. In the W-band (95 GHz) ESR measurement, the Zeeman term dominates the zero-field splitting in the spin Hamiltonian, and the spectrum exhibits a pattern that can be easily assigned. The combined use of a W-band (95 GHz) and X-band (9.5 GHz) spectrometers makes the analysis simple and reliable.

Experimental Section

A highly purified sample of the major isomer of Gd@C_{82} (Gd@C_{82}-I (C_{2v})) was obtained by employing the high performance liquid chromatographic (HPLC) method following the previous report.[31] The solution samples in CS_2 or trichloroben-

* Corresponding author. Telephone: +81-564-55-7330. Fax: +81-564-55-4639. E-mail: kato@ims.ac.jp.
[†] Institute for Molecular Science.
[‡] Nagoya University.
[§] The Graduate University for Advanced Studies.

10.1021/jp035947c CCC: $25.00
Published on Web 11/21/2003

zene (TCB) were degassed with a number of freeze−pump−thaw cycles. The powder sample of the Gd@C_{82} was obtained by drying the CS_2 or TCB solution in the vacuum line. Both samples were sealed in thin-walled quartz tube.

The X- and W-band ESR measurements were performed using a Bruker E500 and a E680 spectrometer, respectively. The temperature was controlled by a helium flow cryostat (Oxford Instruments model ESR910: X-band and CF935: W-band) and a cryostat controller (Oxford Instruments model ITC500). The X-band ESR spectra were measured at 4.0 K, and W-band ESR spectra were measured at 20 and 4.0 K. The temperature for the X-band experiment was calibrated using a silicon diode sensor with a digital thermometer (Lake Shore model DT-470-SD-13−1.4L and model 201).

The spectral simulations were performed by means of hybrid eigenfield methods, in which the resonance fields are obtained directly by the solving the eigenfield equation,[32−35]

$$[h\nu\mathbf{E}\otimes\mathbf{E} - H_D\otimes\mathbf{E} + \mathbf{E}\otimes H_D^*]\mathbf{V} = [H_{eZ}\otimes\mathbf{E} - \mathbf{E}\otimes H_{eZ}^*]\mathbf{V} \quad (1)$$

where H_{eZ}, H_D, **E**, and **V** denote the magnetic field dependent and independent terms of the spin Hamiltonian operator, the unit matrix, and the eigenfunction for the eigenfield equation, respectively. The terms h and ν are the Plank constant and the frequency of the microwave radiation. The signal intensity, I, was defined as follows:[32]

$$I = \frac{\exp(E_m/k_BT) - \exp(E_{m'}/k_BT)}{Z} \times |\mu_B\langle m|H_1|m'\rangle|^2 \quad (2)$$

where H_1 stands for the magnetic field of the microwave radiation, i.e., the term responsible for the magnetic dipole allowed transition. The first and second terms show the Boltzmann population and the transition probability from $|m\rangle$ to $|m'\rangle$ state, whose energies are defined as E_m and $E_{m'}$, on the resonance field. Z, k_B, T, and μ_B denote the partition function, the Boltzmann constant, the temperature, and the Bohr magneton. After obtaining the resonance field by the eigenfield method, the eigen energies of the spin Hamiltonian were calculated to obtain the partition function. The random orientation ESR spectra were defined as the summation of the 32400 orientations of ESR spectra for the **g** tensor. We assumed that the principal axes of the **g** tensor and those of the zero-field splitting tensor were collinear. The simulation program was coded by FORTRAN90 and executed on a SGI2800 (8 CPUs) computer.

Results and Discussion

1. *Concentration Dependence of Gd@C_{82}.* Figure 1 shows the X-band ESR spectra of Gd@C_{82}-I in CS_2 solution as a function of concentration and measured at 4.0 K. The uppermost spectrum corresponds to an extremely diluted CS_2 solution. Also shown at the bottom of Figure 1 is the spectrum from a powder sample of Gd@C_{82}-I. The middle spectra are obtained in CS_2 solutions with different concentrations. In all of the X-band ESR spectra, an asymmetric spectral pattern, i.e., the signals with the large intensity at the lower field side and with the small intensity at the higher field side (which corresponds to lower than $g = 2.00$), was observed. This spectral pattern is typical for systems having a zero-field splitting as large as the microwave energy. The zero-field splitting term is not a perturbation since the zero-field splitting is comparable to the Zeeman energy. As shown in Figure 1, the intensity of the component corresponding to the powder sample increased with increase of concentration. The result strongly suggests the dimerization of Gd@C_{82}-I in CS_2 solution.

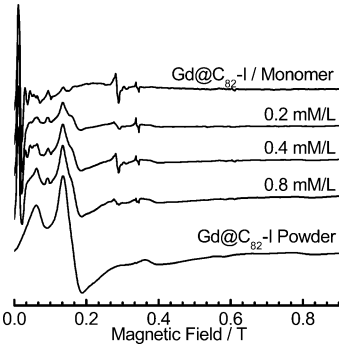

Figure 1. X-band ESR spectra of Gd@C_{82}. Shown in the uppermost spectrum: extremely diluted CS_2 solution; in the bottom spectrum: powder sample. The middle three spectra are CS_2 solutions with different concentrations: 0.2, 0.4, and 0.8 mM/L.

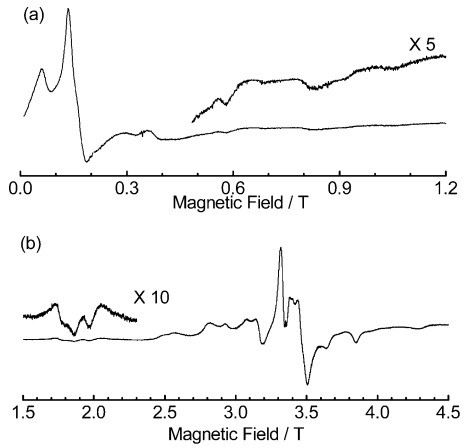

Figure 2. Observed X-band ESR spectrum and W-band ESR spectra at (a) 4.0 K and (b) 20 K for Gd@C_{82} powder, respectively. The microwave frequencies at 20 and 4 K are (a) 9.63973 GHz and (b) 94.1127 GHz.

2. Gd@C_{82} Powder. Figure 2 shows the X-band ESR spectrum of the powder sample recorded at 4.0 K and the W-band ESR spectrum of powder sample recorded at 20 K. The asymmetrical spectral feature recorded using the X-band spectrometer shown in Figure 2a could not be readily simulated. On the other hand, we obtained the symmetrical ESR spectrum with the large signal at $g = 2.00$ in the W-band, as seen in Figure 2b. This result shows that the zero-field splitting is smaller than the W-band microwave energy. To model the spin structure for Gd@C_{82}-I powder, we performed spectral simulation using the following spin Hamiltonian operator,

$$H = \mu_B\mathbf{S}\cdot\mathbf{g}\cdot\mathbf{B}_0 + \mathbf{S}\cdot\mathbf{D}\cdot\mathbf{S} \quad (3)$$

where μ_B, **S**, **g**, $\mathbf{B}_0$, and **D** were described as the Bohr magneton, the spin angular momentum operator, the magnetic **g** tensor, the magnetic field, and the dipole−dipole interaction tensor responsible for the zero-field splitting, respectively. The principal values of the **D** tensor are expressed as $(-D'/3 + E', -D'/3 - E', 2D'/3)$, where D' is the so-called D-term of the zero-field splitting tensor which describes the deviation from the spherical symmetry and E' is the E-term which describes the deviation from the axial symmetry. The higher-order term of the zero-field splitting is neglected. The simulated W-band spectra are shown in Figure 3b. The simulated spectrum is in good agreement with the observed W-band spectrum. The adjustable

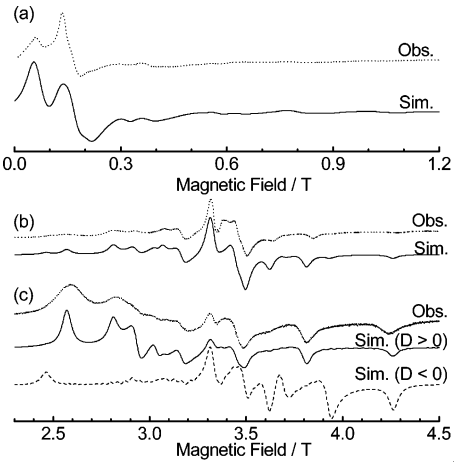

Figure 3. Simulated X-band ESR spectra and W-band ESR spectra at (a) 4.0 K, (b) 20 K, and (c) 4 K for Gd@C_{82} powder, respectively. The solid and broken lines denote the simulated spectra with the positive and negative D value. The dotted line indicates the observed ESR spectrum for Gd@C_{82} powder at 4 K.

parameters used in the simulation were $S = 7/2$, the principal values of the **g** tensor (1.99, 1.99, 2.00), $|D'| = 0.210$ cm^{-1}, and $E' = +0.018$ cm^{-1}. We measured the W-band ESR spectrum at 4 K, to determine the sign of D'. Figure 3c shows the observed W-band ESR spectrum with the simulated spectra for positive and negative D' at 4 K. The calculated spectrum for positive D' is consistent with the observed one at 4 K.

The validity of the ESR parameters derived from modeling the W-band spectrum was confirmed by their ability to simulate the X-band ESR spectrum. Figure 3a shows the simulated spectra for the X-band ESR of Gd@C_{82}-I powder. The simulated spectrum not only reproduced the observed main peaks but also the extra lines. In the powder form, the X- and W-band ESR spectra are characterized by $S = 7/2$, which originates from seven spins on the 4f orbital of Gd^{3+} ion. The spin quantum number $S = 7/2$ is consistent with the dimer formation of Gd@C_{82}-I in solution observed in Figure 1. The radical spins on the cage could be antiparallel coupled in the formation of magnetic dimer, and the resultant spin state of the dimer would be described by two independent octet ($S = 7/2$) spins of Gd^{3+}. The magnetic dimer can be related to the preferential dimer formation of metallofullerenes reported by Hasegawa et al.[30] as mentioned in the Introduction. The intermolecular magnetic interaction between two Gd^{3+} spins in the dimer is smaller than the line width of the ESR spectra in the Gd@C_{82}-I powder.

3. Gd@C_{82} in TCB Solution. As described in the preceding section, the spectrum of Gd@C_{82}-I in diluted solution was attributed to the monomer of Gd@C_{82}-I. To investigate the intrinsic spin state of the molecule of Gd@C_{82}-I, the spectrum in dilute solution without any disturbance from intermolecular interaction, i.e., magnetic dimerization, should be observed. Figure 4 shows the observed W-band ESR spectra for Gd@C_{82} in dilute TCB solution at 4 and 20 K. The symmetrical spectral pattern with center at $g = 2.00$ was observed. Unlike the Gd@C_{82} powder, it exhibits the spectrum without the largest intensity at $g = 2.00$. This spectral pattern is that for the non-Kramers system, which has an integer spin quantum number. The signal intensity around $g = 2$ decreases with decreasing temperature. This feature suggests that the components around $g = 2$ are contributed from the excited spin state.

The spin state of the Gd@C_{82}-I monomer should be described by the total angular momentum of $S_{tot} = 3$ or $S_{tot} = 4$. The total angular momentum results from the coupling between the

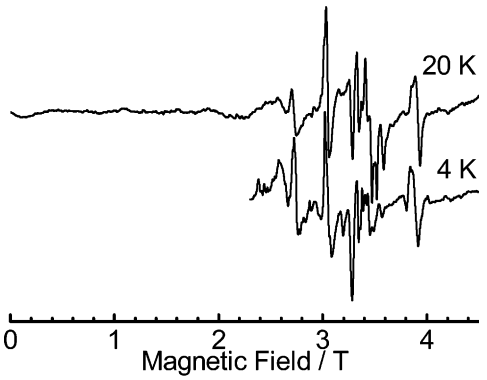

Figure 4. Observed W-band ESR spectra for Gd@C_{82} in TCB solution at 20 and 4 K. The microwave frequency at 20 and 4 K is 94.2382 and 94.0964 GHz, respectively.

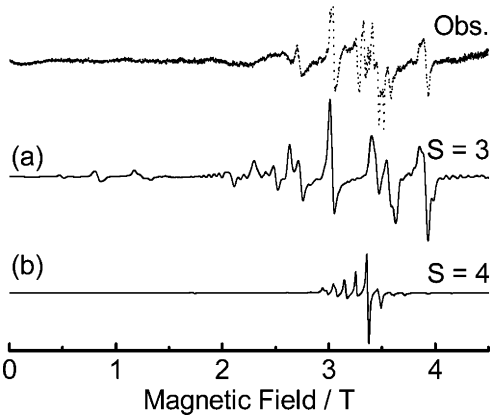

Figure 5. Simulated W-band ESR spectra for (a) $S = 3$ and (b) $S = 4$ by the total angular momentum method. The broken line shows the observed W-band ESR spectrum for Gd@C_{82} in TCB solution at 20 K.

TABLE 1: Spin Hamiltonian Parameters for Gd@C_{82} in TCB Solution Using Total Angular Momentum Method

	$S = 3$	$S = 4$
g	(1.9970 1.9991 1.9676)	(2.0210 2.0209 1.9874)
$D'_{S=n}$/cm^{-1}	+0.4125	+0.1025
$E'_{S=n}$/cm^{-1}	+0.0120	+0.0020

$S = 7/2$ spin on the Gd^{3+} ion and the radical spin ($S = 1/2$) on C_{82}, and the total angular momentum of $S_{tot} = 3$ and $S_{tot} = 4$ are produced by the antiferromagnetic and ferromagnetic couplings, respectively. Some trials of the simulation by using $S_{tot} = 3$ gave a satisfactory spectrum which fitted the observed W-band spectrum, except for the central lines around $g = 2$, as shown in Figure 5a. After an effort to reproduce the central lines around $g = 2$, one set of reasonable parameters could be obtained with the simulation by $S_{tot} = 4$, as shown in Figure 5 b. The parameters obtained by both simulations by $S_{tot} = 3$ and $S_{tot} = 4$ are summarized in Table 1. As mentioned above, the signal intensity around $g = 2$ decreases with decreasing temperature. Therefore, the spin state with $S_{tot} = 4$ is considered to be the excited state. As a result, it is concluded that the observed W-band spectrum is a mixture arising from the ground state of $S_{tot} = 3$ and a thermally excited state of $S_{tot} = 4$.

In the model of the spin structure using the Hamiltonian in eq 3, the intramolecular exchange coupling, J, between two spin sites on the orbital of the fullerene cage ($S_R = 1/2$) and the octet spin ($S_{Gd} = 7/2$) of the encapsulated gadolinium ion, is neglected. This model is valid under the approximation with

TABLE 2: Spin Hamiltonian Parameters for Gd@C_{82} Powder and Gd@C_{82} in TCB Solution

	powder	TCB solution
S_{Gd}	7/2	7/2
S_R	NA	1/2
$\mathbf{g}_{Gd}$	(1.9900 1.9900 2.0000)	(2.0090 2.0100 1.9775)
$\mathbf{g}_R$	NA	(2.1050 2.0970 2.0570)
D'_{Gd}/cm^{-1}	+0.2100	+0.2575
E'_{Gd}/cm^{-1}	+0.0180	+0.0070
D'_{Gd-R}/cm^{-1}	NA	−0.7250
E'_{Gd-R}/cm^{-1}	NA	−0.0260

an infinite value of J. However, for the explicit estimation of J, it is required to convert the basis set of the total angular momentum, S_{tot}, to that of the spin angular momenta S_{Gd} and S_R on both radical sites. Instead of the Hamiltonian in eq 3 for the basis set $|S_{tot},M_{Stot}\rangle$, the following Hamiltonian is appropriate for forming the eigenfunction in the basis set $|S_{Gd},M_S^{Gd}; S_R,M_S^R\rangle$,

$$H = \mu_B(\mathbf{S}_{Gd}\cdot\mathbf{g}_{Gd}\cdot\mathbf{B}_0 + \mathbf{S}_R\cdot\mathbf{g}_R\cdot\mathbf{B}_0) + \mathbf{S}_{Gd}\cdot\mathbf{D}_{Gd}\cdot\mathbf{S}_{Gd} + \mathbf{S}_{Gd}\cdot\mathbf{D}_{Gd-R}\cdot\mathbf{S}_R - 2J\mathbf{S}_{Gd}\cdot\mathbf{S}_R \quad (4)$$

where J denotes the intramolecular exchange coupling parameter between the Gd^{3+} and radical spins, $\mathbf{S}_{Gd}$ and $\mathbf{g}_{Gd}$ stand for the spin operator and the $\mathbf{g}$ tensor for Gd^{3+} ion, and $\mathbf{S}_R$ and $\mathbf{g}_R$ for the radical spin on the C_{82} cage, respectively. $\mathbf{B}_0$ is the magnetic field, $\mathbf{D}_{Gd}$ is the zero-field splitting tensors for Gd^{3+} ion, $\mathbf{D}_{Gd-R}$ is the magnetic dipole−dipole interaction tensor between the Gd^{3+} and the radical spins, respectively. The principal values of the $\mathbf{D}_{Gd-R}$ and $\mathbf{D}_{Gd}$ tensors are expressed as $(-D'_{Gd-R}/3 + E'_{Gd-R}, -D'_{Gd-R}/3 - E'_{Gd-R}, 2D'_{Gd-R}/3)$, and $(-D'_{Gd}/3 + E'_{Gd}, -D'_{Gd}/3 - E'_{Gd}, 2D'_{Gd}/3)$, respectively. The ESR parameters for the basis set of $|S_{tot},M_{Stot}\rangle$ can be converted to that for $|S_{Gd},M_S^{Gd}; S_R,M_S^R\rangle$ by Clebsch−Gordan coefficients. Specifically, The ESR parameters for two basis sets are related each other as follows,[36]

$$\mathbf{g}_{S=n} = c_1\,\mathbf{g}_{Gd} + c_2\,\mathbf{g}_R \quad (5)$$

$$\mathbf{D}_{S=n} = d_1\,\mathbf{D}_{Gd} + d_{12}\,\mathbf{D}_{Gd-R} \quad (6)$$

where $\mathbf{g}_{S=n}$ denotes the $\mathbf{g}$ tensor for $S = n$ ($n = 3$ or 4), $\mathbf{g}_{Gd}$ and $\mathbf{g}_R$ are for the Gd^{3+} ion and the radical on C_{82} cage, respectively. The $\mathbf{D}_{S=n}$ is the fine-structure tensor for $S = n$ ($n = 3$ or 4), $\mathbf{D}_{Gd}$ and $\mathbf{D}_{Gd-R}$ are for the Gd^{3+} ion and between the Gd^{3+} ion and the radical spin on the cage. The factors of c_1, c_2, d_1, and d_{12} are introduced by the substitution of $\mathbf{S}_{Gd}$ and $\mathbf{S}_R$ for $\mathbf{S}_{S=n}$ ($n = 3$ or 4) in the Wigner−Eckart theorem. These factors depend only on S_{tot}, S_{Gd}, and S_R, and are expressed as follows. $S = 3$: $c_1 = 9/8$, $c_2 = -1/8$, $d_1 = 5/4$, and $d_{12} = -1/8$. $S = 4$: $c_1 = 7/8$, $c_2 = 1/8$, $d_1 = 3/4$, and $d_{12} = 1/8$. All ESR parameters for the basis set $|S_{Gd},M_S^{Gd}; S_R,M_S^R\rangle$ except the J were given from the parameters $\mathbf{g}_{S=n}$ and $\mathbf{D}_{S=n}$ in Table 1. They are summarized in Table 2 compared with that for the Gd@C_{82}-I powder. The adjustable parameter J was determined by the spectral simulation as shown in Figure 6. In the case that J equals positive 5.5 cm^{-1}, i.e., the bottom trace in Figure 6a, the spectrum dominated by the $S = 4$ state gives the center structure. As can be seen in the above two figures, the structure on either side of the center originates from the $S = 3$ state and becomes more evident with more negative J. Changing the value of J from -1.8 cm^{-1} to -5.5 cm^{-1}, the intensity of the structure on either side is not drastically altered at 20 K for the W-band measurement, as can be seen in Figure 6a. The simulation of the 4 K W-band measurement is not strongly sensitive to changing the value of J, as shown in Figure 6b. However, the spectrum at 4 K for the X-band measurement, which is shown in Figure 6c, exhibits a keen sensitivity to the value of J. When J is taken to be -1.8 cm^{-1}, there is good agreement between the observed and simulated spectra, see the top and second traces of Figure 6c. Finally, all spectra observed at 4 and 20 K in the W-band and at 4 K in the X-band experiments were well reproduced by the simulation using eq 4 with the exchange coupling $J = -1.8$ cm^{-1}. The negative sign of J means that the Gd spin is antiferromagnetically coupled with the radical spin on C_{82} cage. It can be concluded that the spin state of $S = 3$ is the ground state and that the energy difference with the excited state of $S = 4$ is 14.4 cm^{-1} (the energy gap is described by "8J"). It is noted that the principal values of $\mathbf{g}_{Gd}$ and $\mathbf{D}_{Gd}$ tensor do not exactly coincide with those for Gd@C_{82}-I powder, and the principal value of the $\mathbf{g}_R$ tensor on the radical site of the cage deviates from the value of $g = 2.00$, which is usually expected for an organic radical.[31] The total symmetry of the Gd@C_{82}-I molecule is thought to be C_{2v} based on comparison with the La@C_{82}-I (C_{2v}) data,[23] as mentioned before. The principal axes of the dipole−dipole interaction, $\mathbf{g}_{Gd}$, and $\mathbf{g}_R$ tensors are parallel, and the tensors have C_{2v} symmetry. The negative sign and magnitude of the D_{Gd-R} parameter can be obtained by the estimates of the dipole−dipole interaction between the Gd ion and the radical electron cloud on the C_{82} cage, as will be reported elsewhere.

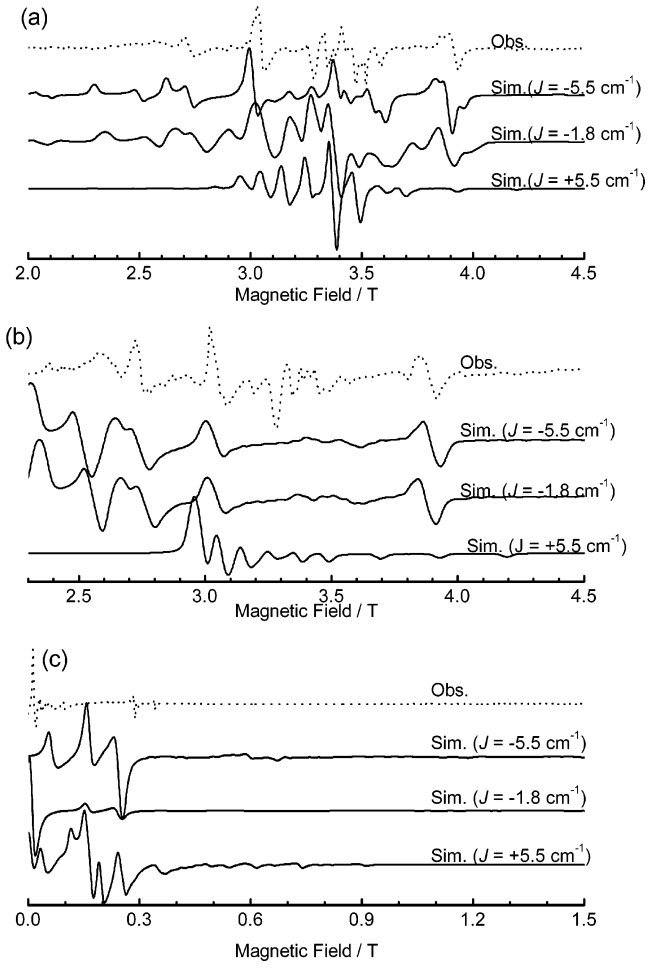

Figure 6. Simulated ESR spectra for $J = -5.5$ cm^{-1}, -1.8 cm^{-1}, and $+5.5$ cm^{-1} by the exact spin Hamiltonian method at (a) 20 K in the W-band, (b) 4 K in the W-band, and (c) 4 K in the X-band, respectively. The dotted line indicates the observed W-band ESR spectrum for Gd@C_{82} in TCB solution.

Conclusion

The magnetic properties for Gd@C_{82}-I were examined in terms of X- and W-band ESR spectroscopy. We recorded the W-band ESR spectra of Gd@C_{82}-I in powder form and in solution of CS_2 and TCB. To reveal the spin structure for Gd@C_{82}-I, spectral simulations were performed by means of the eigenfield method. In powder form, both X- and W-band ESR spectra were reproduced by ensuring the spin state of $S = 7/2$, which resulted from the magnetic dimer formation. On the other hand, the observed W-band ESR spectrum for Gd@C_{82}-I monomer in a TCB solution was well explained by the antiferromagnetically intramolecular exchange coupling between $S_{Gd} = 7/2$ and $S_R = 1/2$. The exchange coupling parameter $J = -1.8$ cm^{-1} was determined by the simulation. In other words, the spectrum of the Gd@C_{82}-I monomer was assigned to the mixed spin states of the ground $S = 3$ and the thermally excited $S = 4$ states, whose energy gap was 14.4 cm^{-1}. This is the first report of the quantitative estimation of the magnetic interaction between the metal ion and the radical spin on the cage in a metallofullerene.

Acknowledgment. The authors thank the Research Center for Computational Science, Okazaki National Research Institutes for the use of The SGI 2800 computer. Thanks are due to the Research Center for Molecular-Scale Nanoscience, the Institute for Molecular Science for assistance in obtaining the W-band ESR spectra.

References and Notes

(1) Hino, S.; Umishita, K.; Iwasaki, K.; Aoki, M.; Kobayashi, K.; Nagase, S.; Dennis, T. J. S.; Nakane, T.; Shinohara, H. *Chem. Phys. Lett.* **2001**, *337*, 65−71.

(2) Krause, M.; Kuran, P.; Kirbach, U.; Dunsch, L. *Carbon* **1999**, *37*, 113−115.

(3) Bethune, D. S.; Johnson, R. D.; Salem, J. R.; Devries, M. S.; Yannoni, C. S. *Nature* **1993**, *366*, 123−128.

(4) Beyers, R.; Kiang, C. H.; Johnson, R. D.; Salem, J. R.; Devries, M. S.; Yannoni, C. S.; Bethune, D. S.; Dorn, H. C.; Burbank, P.; Harich, K.; Stevenson, S. *Nature* **1994**, *370*, 196−199.

(5) Johnson, R. D.; Devries, M. S.; Salem, J.; Bethune, D. S.; Yannoni, C. S. *Nature* **1992**, *355*, 239−240.

(6) Lee, J.; Kim, H.; Kahng, S. J.; Kim, G.; Son, Y. W.; Ihm, J.; Kato, H.; Wang, Z. W.; Okazaki, T.; Shinohara, H.; Kuk, Y. *Nature* **2002**, *415*, 1005−1008.

(7) Shinohara, H.; Sato, H.; Ohkohchi, M.; Ando, Y.; Kodama, T.; Shida, T.; Kato, T.; Saito, Y. *Nature* **1992**, *357*, 52−54.

(8) Takata, M.; Umeda, B.; Nishibori, E.; Sakata, M.; Saito, Y.; Ohno, M.; Shinohara, H. *Nature* **1995**, *377*, 46−49.

(9) Wang, C. R.; Kai, T.; Tomiyama, T.; Yoshida, T.; Kobayashi, Y.; Nishibori, E.; Takata, M.; Sakata, M.; Shinohara, H. *Nature* **2000**, *408*, 426−427.

(10) Kato, T.; Bandou, S.; Inakuma, M.; Shinohara, H. *J. Phys. Chem.* **1995**, *99*, 856−858.

(11) Shinohara, H.; Sato, H.; Saito, Y.; Ohkohchi, M.; Ando, Y. *J. Phys. Chem.* **1992**, *96*, 3571−3573.

(12) Shinohara, H.; Hayashi, N.; Sato, H.; Saito, Y.; Wang, X. D.; Hashizume, T.; Sakurai, T. *J. Phys. Chem.* **1993**, *97*, 13438−13440.

(13) Shinohara, H.; Yamaguchi, H.; Hayashi, N.; Sato, H.; Ohkohchi, M.; Ando, Y.; Saito, Y. *J. Phys. Chem.* **1993**, *97*, 4259−4261.

(14) Shinohara, H.; Inakuma, M.; Hayashi, N.; Sato, H.; Saito, Y.; Kato, T.; Bandow, S. *J. Phys. Chem.* **1994**, *98*, 8597−8599.

(15) Shinohara, H. *Rep. Prog. Phys.* **2000**, *63*, 843−892.

(16) Kato, H.; Suenaga, K.; Mikawa, W.; Okumura, M.; Miwa, N.; Yashiro, A.; Fujimura, H.; Mizuno, A.; Nishida, Y.; Kobayashi, K.; Shinohara, H. *Chem. Phys. Lett.* **2000**, *324*, 255−259.

(17) Mikawa, M.; Kato, H.; Okumura, M.; Narazaki, M.; Kanazawa, Y.; Miwa, N.; Shinohara, H. *Bioconjugate Chem.* **2001**, *12*, 510−514.

(18) Hirahara, K.; Suenaga, K.; Bandow, S.; Kato, H.; Okazaki, T.; Shinohara, H.; Iijima, S. *Phys. Rev. Lett.* **2000**, *85*, 5384−5387.

(19) Suenaga, K.; Tence, T.; Mory, C.; Colliex, C.; Kato, H.; Okazaki, T.; Shinohara, H.; Hirahara, K.; Bandow, S.; Iijima, S. *Science* **2000**, *290*, 2280−2282.

(20) Akasaka, T.; Nagase, S.; Kobayashi, K. *J. Synth. Org. Chem. Jpn.* **1996**, *54*, 580−585.

(21) Shinohara, H. *Sci. Rep. Res. Inst. Tohoku University Ser. A-Phys. Chem. Metall.* **1997**, *44*, 47−50.

(22) Liu, S. Y.; Sun, S. Q. *J. Organomet. Chem.* **2000**, *599*, 74−86.

(23) Akiyama, K.; Sueki, K.; Kodama, T.; Kikuchi, K.; Ikemoto, I.; Katada, M.; Nakahara, H. *J. Phys. Chem. A* **2000**, *104*, 7224−7226.

(24) Suenaga, K.; Iijima, S.; Kato, H.; Shinohara, H. *Phys. Rev. B* **2000**, *62*, 1627−1630.

(25) Funasaka, H.; Sakurai, K.; Oda, Y.; Yamamoto, K.; Takahashi, T. *Chem. Phys. Lett.* **1995**, *232*, 273−277.

(26) Funasaka, H.; Sugiyama, K.; Yamamoto, K.; Takahashi, T. *J. Phys. Chem.* **1995**, *99*, 1826−1830.

(27) Huang, H. J.; Yang, S. H.; Zhang, X. X. *J. Phys. Chem. B* **1999**, *103*, 5928−5932.

(28) Huang, H. J.; Yang, S. H.; Zhang, X. X. *J. Phys. Chem. B* **2000**, *104*, 1473−1481.

(29) Sanakis, Y.; Tagmatarchis, N.; Aslanis, E.; Ioannidis, N.; Petrouleas, V.; Shinohara, H.; Prassides, K. *J. Am. Chem. Soc.* **2001**, *123*, 9924−9925.

(30) Hasegawa, Y.; Ling, Y.; Yamazaki, S.; Hashizume, T.; Shinohara, H.; Sakai, A.; Pickering, H. W.; Sakurai, T. *Phys. Rev. B* **1997**, *56*, 6470−6473.

(31) Okubo, S.; Kato, T.; Inakuma, M.; Shinohara, H. *New Diamond Front. Carbon Technol.* **2001**, *11*, 285−294.

(32) Takui, T.; Matsuoka, H.; Furukawa, K.; Nakazawa, S.; Sato, K.; Shiomi, D. In *EPR of Radicals in Solids: Trends in Methods and Applications*; Lund, A., Shiotani, M., Eds.; Kluwer Academic Publishers: Dordrecht, 2003.

(33) McGregor, K. T.; Scaringe, R. P.; Hatfield, W. E. *Mol. Phys.* **1975**, *30*, 1925−1933.

(34) Belford, R. L.; Belford, G. G. *J. Chem. Phys.* **1973**, *59*, 853−854.

(35) Belford, G. G.; Belford, R. L.; Burkhalt, J. F. *J. Magn. Reson.* **1973**, *11*, 251−265.

(36) Bencini, A.; Gatteschi, D. *EPR of Exchange Coupled Systems*; Springer-Verlag: Berlin, 1989.